A Multi-Ion, Flux-Corrected Transport Based Hydrodynamic Model for the Plasmasphere Refilling Problem

K. Chatterjee[1,2], and R.W. Schunk[3].

[1] Geospace Physics Laboratory, NASA, Goddard Space Flight Center, Greenbelt, MD 20771

[2]Department of Electrical and Computer Engineering, University of New Mexico, Albuquerque, NM 87131

[3]Center for Atmospheric and Space Sciences, Utah State University, Logan, UT 84322

Corresponding author: Kausik Chatterjee (kausik.chatterjee@nasa.gov, kchatterjee@unm.edu, kausik.chatterjee@aggiemail.usu.edu)

Key Points:

- Developed a hydrodynamic model for the plasmasphere refilling problem following geomagnetic storms.
- The model is based on the well-known flux-corrected transport method.
- The model is applied to the plasmasphere refilling problem for three ion species and two neutrals along the L = 4 line.

Abstract

The objective of this paper is the application of a newly-developed Flux-Corrected Transport (FCT) based hydrodynamic solution methodology to the plasmasphere refilling problem following a geomagnetic storm. The FCT method is extremely well-suited to the solution of nonlinear partial differential equations with shocks and discontinuities. In this solution methodology, every ion species is modeled as two separate fluids originating from the northern and southern hemispheres. We present refilling results that includes three ion (H^+, He^+ and O^+) species and two neutrals (H and O). We believe that with additional modifications, the model can be adapted to the solution of other ionosphere-magnetosphere coupling problems.

Plain Language Summary

The paper applies a newly-developed multi-species hydrodynamic model to the plasmasphere refilling problem following geomagnetic storms. We believe that with additional development, the model can be applied to other ionosphere-magnetosphere problems.

1 Introduction

A geomagnetic storm [*Gonzalez et al.,* 1994] is a temporary disturbance of the Earth's magnetosphere caused by a solar wind shock wave that interacts with the Earth's magnetic field. Several space weather related phenomena are linked to geomagnetic storms, including but not restricted, to solar energetic particle (SEP) events [*Reames,* 2017], geomagnetically induced currents [*Pirjola,* 2000] and ionospheric disturbances that lead to radio and radar scintillation [*Edde,* 1992]. Consequently, geomagnetic storms affect high-frequency radio communication, satellite navigation and power grids, and thus, a very active area of research.

The plasmasphere [*Gringauz,* 1963; *Goldstein et al.,* 2002; *Sandel et al.,* 2003; *Millian & Thorne,* 2007; *Darrouzet et al.,* 2009] is the lowermost region of the magnetosphere and lies just above the ionosphere. It has been traditionally described [*Rasmussen & Schunk,* 1988] as a toroidal-shaped mass of cold plasma (about 1 ev in energy), co-rotating with the earth. Following a geomagnetic storm [*Singh et al.,* 1986; *Rasmussen & Schunk,* 1988], the flux tubes linked to the outer layers of the plasmasphere are peeled away from the region. These flux tubes are then convected to the magnetopause in the sunward direction, where they lose the plasma contained within them. The removal of plasma from the outer layers of the plasmasphere in turn, causes the plasmapause to shift to lower magnitude latitudes. As the geomagnetic storm subsides, magnetospheric convection

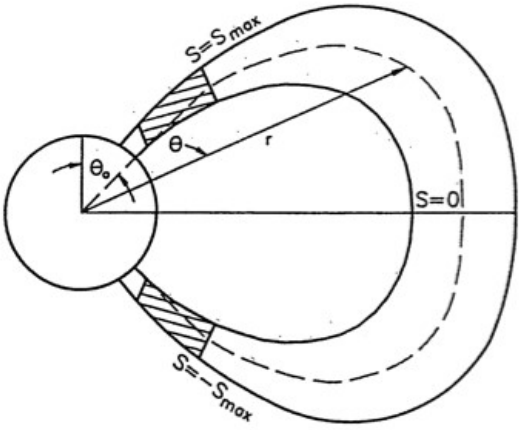

Figure 1. A depleted flux tube: The ionosphere is shown in hatched lines. The ionosphere is embedded in the neutral atmosphere and above the ionosphere is the depleted flux tube immediately after a geomagnetic storm [*Rasmussen & Schunk,* 1988].

returns to its pre-storm level, leaving the plasma density in the outer layers of the plasmasphere significantly depleted. The resultant pressure gradient causes the ionospheric plasma to flow upward along the flux tube, which initiates the process of refilling of the outer layers of the plasmasphere. A schematic diagram of the flux tube is shown in Figure 1.

The plasmasphere plays a critical role in space weather [*Toth et al.,* 2005] as it mediates the wave-particle interactions [*Gendrin,* 1975] in the inner magnetosphere which is crucial to understanding spacecraft charging [*Garrett,* 1981]. Additionally, cold, dense plasmaspheric plumes are expected to substantially impact dayside magnetic reconnection [*Scholer*, 1989]. As a broader point, there is a general understanding [*Rasmussen & Schunk,* 1988] within the community of space physicists and model developers, that the spatial variation of the geomagnetic field within the plasmaspheric flux tubes is relatively well-behaved compared to other locations within the Ionosphere-Magnetosphere system, and as a result, the physical insights gleaned from these modeling studies can indeed prove to be useful in the study of other space plasma transport problems. As a result, the modeling of plasmaspheric refilling after a storm is an important problem.

Over the last several decades, a multitude of studies have been undertaken to model and quantify plasma transport between the ionosphere and the plasmasphere and these studies have led to the development of several ionosphere-plasmasphere coupling models. These models, based on the numerical solution of the plasma transport equations, fall within two broad categories. In the first category (known as the 'diffusion model'), the nonlinear inertial terms in the plasma transport equations are neglected and thus only low-speed, diffusion-dominated flow can be modeled. Included in this category of models are the Sheffield University Plasmasphere Ionosphere Model (SUPIM) [*Bailey, et al.,* 1997], the Ionosphere-Plasmasphere Model (IPM) [*Schunk et al.,* 2004], and the Field-Line Interhemispheric Plasma (FLIP) model [*Young et al.*, 1980]. The FLIP model has recently been assimilated into the Ionosphere Plasmasphere Electrodynamics (IPE) model [*Maruyuma et al.,* 2016] developed at National Oceanic and Atmospheric Administration/Space Weather Prediction Center (NOAA/SWPC) to facilitate an improved understanding of the relation between terrestrial and space weather.

The second category of models that exists in the literature is the so-called 'hydrodynamic model,' where the nonlinear inertial terms are retained in the plasma transport equations. The hydrodynamic model was first introduced by *Banks et al.* [1971] and has subsequently been used by many scientists and researchers working in the field, including *Khazanov et al.* [1984], *Singh et al.* [1986] and *Rasmussen & Schunk* [1988]. The most well-developed hydrodynamic model of the low-latitude ionosphere is SAMI2, developed by *Huba & Joyce* [2000]. Based on the SAMI2 formulation, a 3D global ionosphere code SAMI3 has been developed and has been applied to the plasmasphere refilling [*Krall & Huba,* 2013] problem.

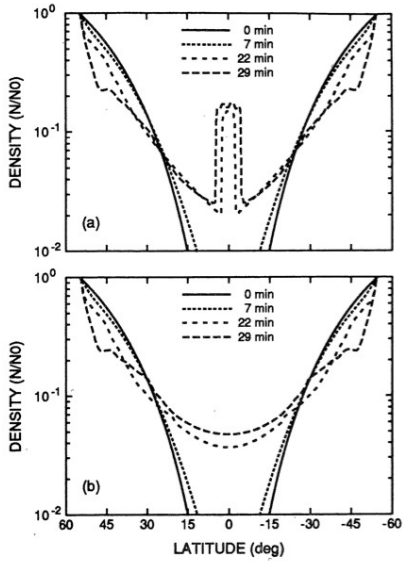

Figure 2. Comparison of single stream (top) and two-stream (bottom) models. Figure 2a (Top panel): Formation of equatorial shock obtained from the "single-stream" model at the onset of refilling [*Singh et al.*, 1986]. Figure 2b (Bottom panel): Absence of equatorial shock obtained from the "two-stream" model at the onset of refilling [*Rasmussen & Schunk*, 1988].

These theoretical models, along with experimental observations that went to validating these models, produced three basic features:

A. Fast, supersonic outflow of H^+ ions from the conjugate ionospheres during the early hours of refilling.
B. Counter-streaming of these H^+ ions, also observed during these early hours.
C. A state of diffusive equilibrium that is reached when the two ion streams are thermalized and there is a decrease from the supersonic velocities reached during the early stages.

The fundamental objective of this paper is the development of a hydrodynamic plasmasphere refilling model, based on the well-known flux corrected transport (FCT) method of *Boris & Book* [1976], which is extremely well-suited to problems with shocks and discontinuities. The FCT method has previously been used (for the H^+ species) in *Singh et al.* [1986] and *Rasmussen & Schunk* [1988]. In *Singh et al.* [1986], the plasma corresponding to a given species was modeled as a single stream of plasma, which led to the formation of unphysical shocks at the equator when plasma originating from the conjugate hemispheres first reached the equator. On the other hand, in *Rasmussen & Schunk* [1988], the same plasma was modeled as two separate streams originating

from the conjugate hemispheres, which led to the interpenetration of streams at the equator and remedied the problem of unphysical shock formation.

This FCT-based two-stream solution methodology presented here is developed independently of *Rasmussen & Schunk* [1988], and it includes three ion species (H^+, O^+ and He^+) and two neutral atoms (*H* and *O*). It should be borne in mind that the competing models and methodologies described previously [*Bailey, et al.,* 1997; *Schunk et al.,* 2004; *Young et al.,* 1980; *Singh et al.,* 1986; *Krall & Huba,* 2013] are single-stream models. The model presented here is philosophically different on the issue of shock formation at the equator and thus likely to give different qualitatively different results in the early to middle stages of refilling. We now provide a brief description of the formulation of the refilling problem.

2 The Plasmasphere Refilling Problem: A Brief Formulation

We begin with the time-dependent continuity and momentum equations for a given ion species indicated by the suffix *i* [*Rasmussen & Schunk,* 1988; *Schunk & Nagy,* 2009], but we re-write the equations with the terms related to the cross-sectional area of flux tube on the right-hand side of the equations:

$$\frac{\partial n_i}{\partial t} + \frac{\partial}{\partial s}(n_i u_i) = -n_i u_i \frac{1}{A}\frac{\partial A}{\partial s} \tag{1a}$$

$$\frac{\partial (n_i u_i)}{\partial t} + \frac{\partial n_i u_i^2}{\partial s} = -(n_i u_i^2)\frac{1}{A}\frac{\partial A}{\partial s} - \frac{1}{m_i}\frac{\partial p_i}{\partial s} + \frac{q n_i}{m_i}E(s) - n_i g(s) + \sum_j n_i \nu_{ij}(u_j - u_i)\varphi_{ij} \tag{1b}$$

where *t* is time, *s* is the spatial coordinate along the magnetic field line, n_i is the ion concentration with each species being represented by two streams, *q* is the ion charge, u_i is the ion drift velocity, *A* is the cross section of the flux tube [*Schunk & Nagy,* 2009], m_i is the ion mass, $p_i = n_i kT$ is the partial ion pressure, *T* is the constant temperature along the flux tube, *k* is the Boltzmann constant, *E* is the electric field, *g*(*s*) is the spatially-dependent gravitational force along the field line, ν_{ij} is the momentum transfer collision frequency and φ_{ij} is a velocity-dependent correction factor [*Rasmussen & Schunk,* 1988; *Schunk & Nagy,* 2009], where '*j*' represents any other ion or neutral species, that is different from '*i*.'

In Equations (1a) and Eq. (1b), the curvature of the dipole magnetic [*Schunk & Nagy,* 2009] field line is accommodated by the two area-dependent source terms in the continuity and momentum conservation equations. The spatially-dependent gravitational force is a function of *h* (the altitude from the earth's surface), *R* (the radius of the earth) and θ (the angle between the radial vector and the magnetic axis), and can be written as:

$$g(s) = 9.8\left(\frac{h}{R+h}\right)^2 \frac{2\cos\theta}{(1+3\cos^2\theta)^{1/2}} ms^{-2}. \tag{2}$$

The expression given above is obtained by taking a scalar product of the gravity vector (which is directed radially) and a unit vector along the dipole magnetic field line given in *Schunk & Nagy* [2009]. Further, imposing quasi-neutrality gives rise to $\sum n_i = n_e$, and neglecting the electron mass in the electron momentum equation gives rise to an expression for the electric field given by

$$E = -\frac{kT}{e\sum n_i}\frac{\partial(\sum n_i)}{\partial s} \quad (3)$$

where *e* is the absolute value of the electronic charge. The expression for electric field provided in Eq. (3), is substituted in Eq. (1b) to obtain a form of the ion momentum equation, where n_i and u_i are the only two unknown variables.

As mentioned before, the plasma transport equations were solved by a solution methodology developed using the well-known flux-corrected transport method pioneered by *Boris & Book* [1976] and developed over the years by several researchers working in the field [*Kuzmin et al.,* 2012; *Otto.,* 2012]. In this paper, the refilling results for the L=4 magnetic field line, are presented, and these results involve three ions (H^+, O^+, He^+) and two neutral (*O, H*) species. The model includes both long-range (ion-ion) and short-range (ion-neutral) collisions [*Schunk & Nagy,* 2009]. For ion-neutral collisions, both resonant and non-resonant collisions [*Schunk & Nagy,* 2009] are included in the model.

The following ion concentrations are assumed at a base altitude of 500 km: $N(O^+) = 2\times10^3\,cm^{-3}$, $N(H^+) = 10^3\,cm^{-3}$ and $N(He^+) = 0.2cm^{-3}$. An initial concentration of $10^{-4}\ cm^{-3}$is assumed for the entirety of the flux tube for all three species and the initial drift velocity is assumed to be zero.

The ion and electron temperatures were both assumed [*Rasmussen & Schunk,* 1988] to be 3560 K [0.3 ev] throughout the entirety of the field line. This allowed the validation of the solution methodology with an exact analytical solution [*Rishbeth & Garriott,* 1969] at steady-state, and the results will be provided in the following section. The neutral temperature was assumed to be 1463 K [0.13 ev], a value reported in *Schunk & Nagy* [2009], obtained from the MSIS model [*MSIS-E-90 Atmosphere Model,* 1990] of terrestrial neutral parameters (Noon, 45° N, 0° E, $F_{10.7}$ = 220, Summer, Altitude - 500 km).

3 Discussion of Results

In this section, the refilling results are presented for time periods extending from 20 minutes to 40 hours. In Figure 3a, we present the hydrogen concentration 20 minutes after the onset of refilling, normalized to the oxygen concentration (as oxygen is the dominant species at the onset of refilling) at the boundaries. The plasmasphere begins to fill up and we observe interpenetration of the streams originating from the northern and southern hemispheres, but no shocks are observed in the middle, consistent with *Rasmussen & Schunk* [1988].

At the end-points reached by either stream, a discontinuity is observed, which is expected. A lot less obvious is a bump in each stream at the domain boundary it is headed to, which is a result of the coupling between the streams, stemming from the electric field term in the transport equations. The origin of these structures is electrostatic in nature. The electric field seen by each stream is affected by the concentration gradient in five other streams, as can be seen from Eq. (3). These discontinuities are realistic subject to the validity of the Maxwellian distribution function [*Schunk & Nagy,* 2009] and the resultant applicability of the plasma transport equations [*Schunk & Nagy,* 2009]. However, in the early to the middle stages of refilling for the L = 4 line, because of the low number densities, the assumption of Maxwellian distribution function might not be valid, in which case the presence or absence of these discontinuities must be explored using a kinetic model [*Wang et al.,* 2015].

In Figure 3b, the hydrogen ion drift velocity profile is presented at 20 minutes after the onset of refilling. High supersonic velocities (thermal velocity $\rightarrow \sqrt{kT/m_i} \rightarrow 5.4\, km/s$) are observed up to the endpoints reached by either stream. These supersonic beams are created as a result of the pressure gradient and the ambipolar electric field.

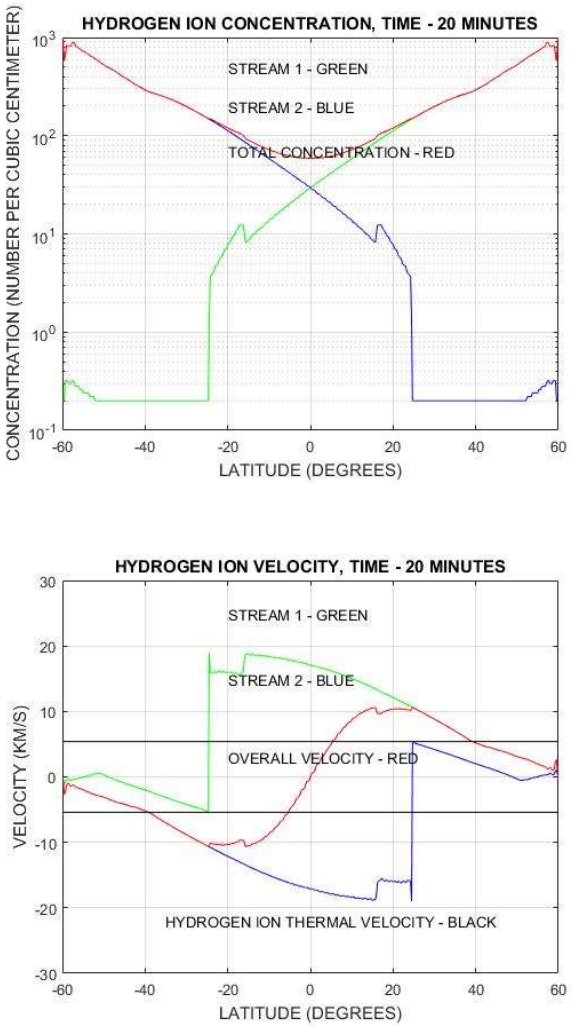

Figure 3a (Top panel). Hydrogen ion concentration profile after 20 minutes. Stream 1 is from the northern hemisphere and stream 2 is from the southern hemisphere. Figure 3b (Bottom panel). Hydrogen ion velocity profile after 20 minutes. The thermal velocity of the hydrogen ions is shown by the horizontal line. Velocities from the northern to the southern hemisphere are taken to be positive.

Based on Eq. (1b), the force due to the pressure gradient per unit volume on a given stream i can be seen to be equal to

$$f_{pi} = -kT\frac{\partial n_i}{\partial s}\,. \tag{4a}$$

Based on Eq. (1b) and Eq. (3), the force due to the electric field per unit volume on the same stream is given by

$$f_{ei} = -\left(\frac{n_i}{\sum n_i}\right) kT \frac{\partial(\sum n_i)}{\partial s}. \tag{4b}$$

Beyond the endpoints reached by either stream, the velocity profile is determined largely by the force of gravity, which on a given stream has accelerating effect in one hemisphere and retarding effect in the other. The total plasma velocity averaged over the contributions of both the streams is also seen to reach supersonic velocities. The concentration bumps at domain boundaries in Figure 3a show corresponding velocity spikes in Figure 3b.

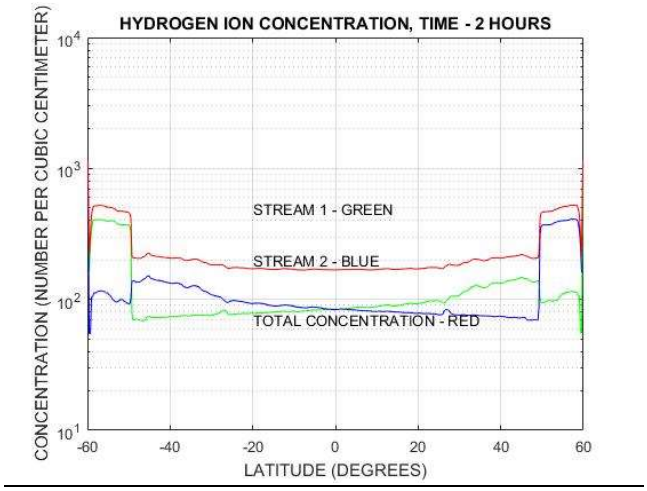

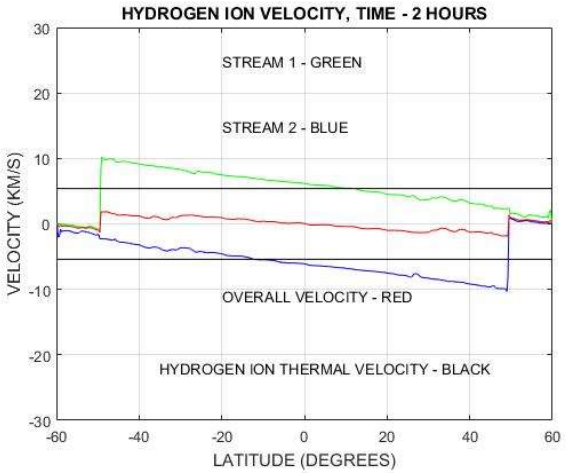

Figure 4a (Top panel). Hydrogen ion concentration profile after 2 hours. Stream 1 is from the northern hemisphere and stream 2 is from the southern hemisphere. Figure 4b (Bottom panel). Hydrogen ion velocity profile after 2 hours. The thermal velocity of the hydrogen ions is shown by the horizontal line. Velocities from the northern to the southern hemisphere are taken to be positive.

In Figure 4a, the hydrogen concentration profile 2 hours after the onset of refilling is presented. The discontinuities in the concentration profile move back and forth as the plasmasphere refills. A discontinuity in the concentration profile of any one stream belonging to a given species, changes the E-field [*See* Eq. (3)], and hence, brings changes in the concentration profile of any other stream, belonging to any other species.

In Figure 4b, the hydrogen velocity profile at 2 hours after the onset of refilling is presented. The individual stream velocities are still supersonic, but equally important is the fact that spatial gradients in the velocity profile are significant at some locations. Due to these discontinuities in the concentration profile, the individual stream velocities, as well as the overall velocity profile, exhibit oscillations throughout the refilling process. But the overall trend is towards subsonic profiles.

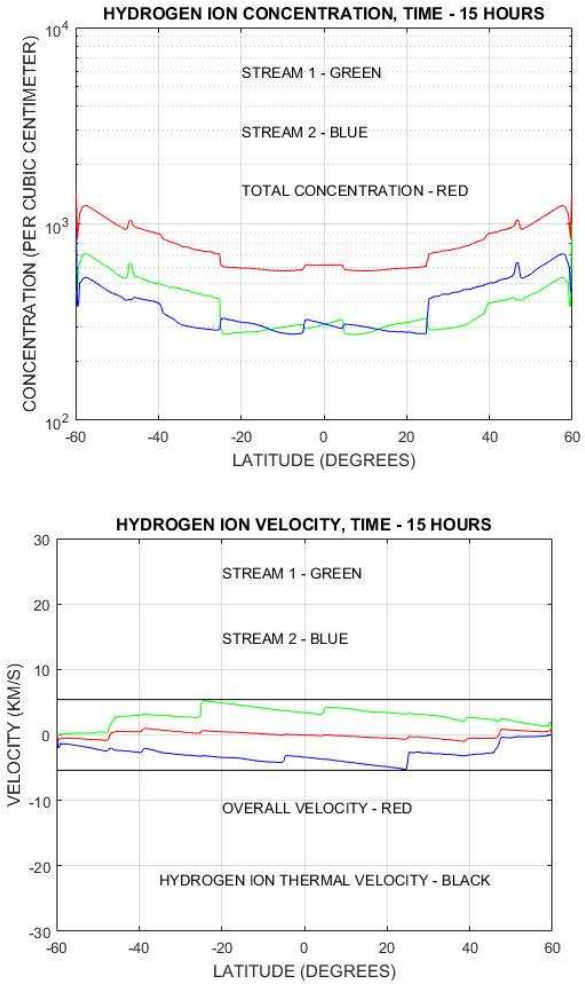

Figure 5a (Top panel). Hydrogen ion concentration profile after 15 hours. Stream 1 is from the northern hemisphere and stream 2 is from the southern hemisphere. Figure 5b (Bottom panel). Hydrogen ion velocity profile after 15 hours. The thermal velocity of the hydrogen ions is shown by the horizontal line. Velocities from the northern to the southern hemisphere are taken to be positive.

In Figure 5a, we present the hydrogen concentration profile at 15 hours after the onset of refilling. We see that the total hydrogen concentration has risen significantly, in that the equatorial concentration is one order of magnitude higher than that at 20 minutes. But the discontinuities are still present and diffusive equilibrium has not yet been reached.

In Figure 5b, the hydrogen velocity profile at 15 hours after the onset of refilling is presented. The stream velocities and the overall plasma velocities are subsonic everywhere along the flux tube.

But it can also be noted that even though the drift velocity is subsonic everywhere, the gradient of the drift velocity is still significant at many points within the spatial domain. This clearly shows the need for hydrodynamic modeling as opposed to diffusion-based modeling after a long time following the onset of refilling.

In Figure 6a, we present the hydrogen ion concentration profile after 40 hours of refilling. Steady-state has almost been reached, and the north and south streams are seen to be close to their diffusive equilibrium states. More importantly, the total hydrogen ion concentration closely matches the analytical solution obtained assuming an infinite flux line [*Rishbeth & Garriott,* 1969].

In Figure 6b, the hydrogen velocity profile after 40 hours of refilling is presented, and it is observed that the stream velocities, the overall velocities and velocity gradients are almost equal to zero, which again is a confirmation of the fact that at 40 hours the refilling process is close to reaching the steady-state.

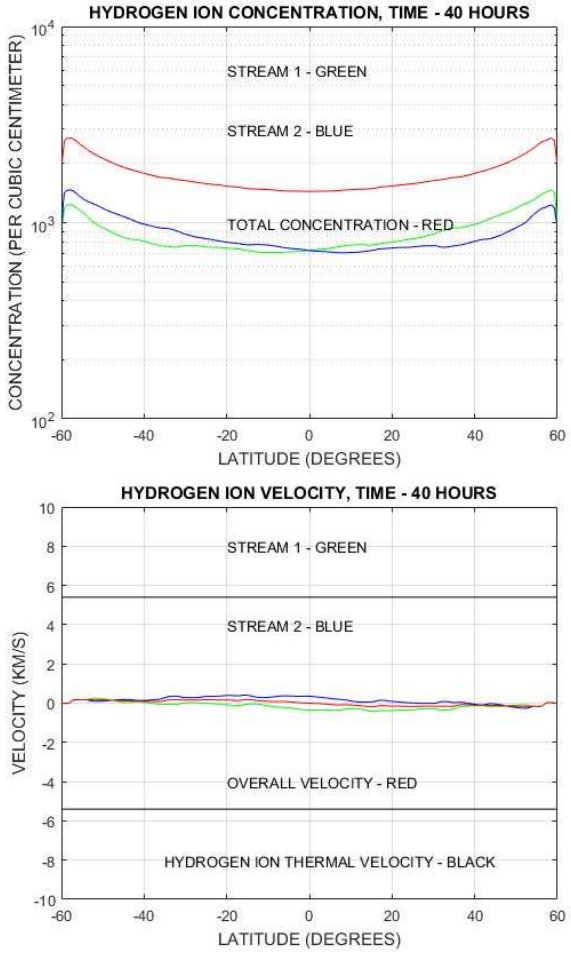

Figure 6a (Top panel). Hydrogen ion concentration after 40 hours. Stream 1 is from the northern hemisphere and stream 2 is from the southern hemisphere. Figure 6b (Bottom panel). Hydrogen ion velocity profile after 40 hours. The thermal velocity of the hydrogen ions is shown by the horizontal line. Velocities from the northern to the southern hemisphere are taken to be positive.

In Figure 7a, we show the helium concentration profile after 40 hours of refilling and in Figure 7b, we show the oxygen concentration profile after the same 40 hours. Comparing Figure 6a to Figure 7b, it can be observed that as we go from the plasmasphere base to higher altitudes along the flux tube, there is an O^+ to H^+ transition. At the plasmasphere base altitude of 500 km at the onset of refilling, O^+ dominates H^+ by a factor of 2:1, which changes to a state of H^+ dominance at the equatorial plane plane by orders of magnitude after 40 hours. Also, as observed from Figure 7a and Figure 7b, after 40 hours, He^+ dominates O^+ for almost the entire flux tube by virtue of its relatively lighter mass.

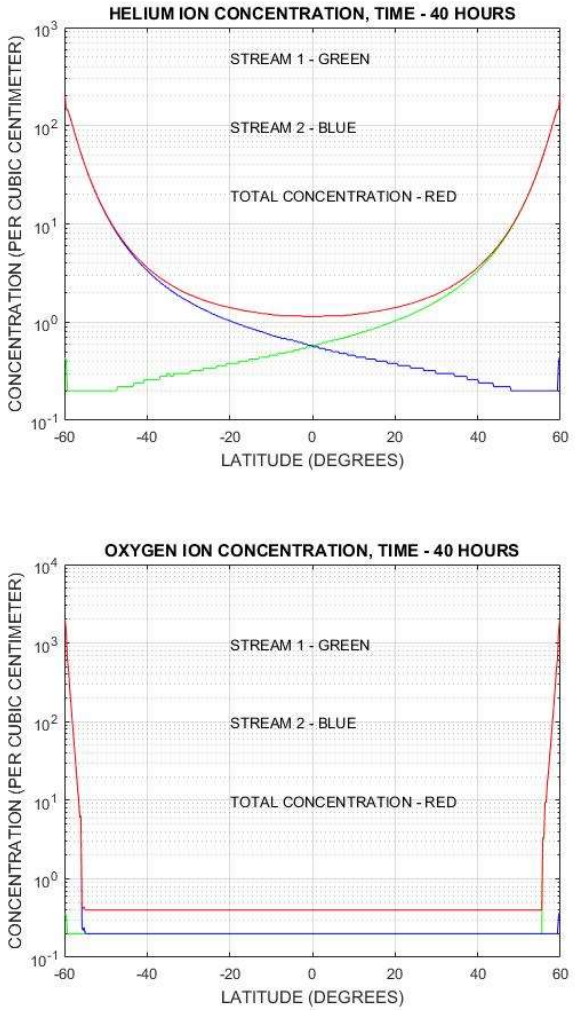

Figure 7a (Top panel). Helium ion concentration profile after 40 hours. Figure 7b (Bottom panel). Oxygen ion concentration profile after 40 hours. Stream 1 is from the northern hemisphere and stream 2 is from the southern hemisphere.

In Figure 8a, we present the equatorial concentration for all three ions as a function of time and we observe that at 40 hours, the plasmasphere is close to reaching a state of diffusive equilibrium. But it also must be borne in mind that our model did not accommodate diurnal ionospheric variations. If instead, we included the diurnal variations and simulated, for example, the boundary conditions for summer and winter solstices, we would expect to see an even more dynamic plasmasphere.

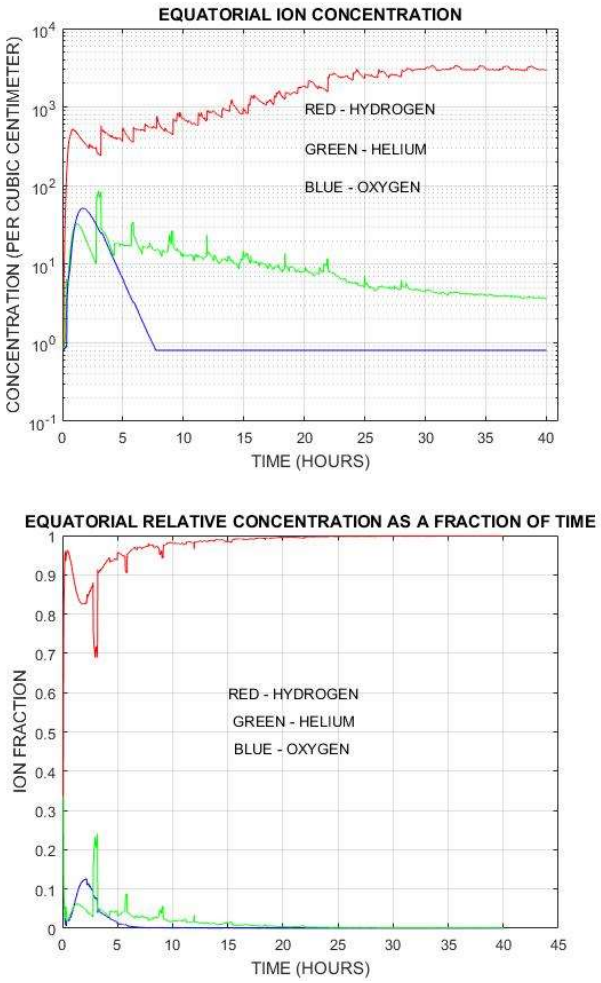

Figure 8a (Top panel). Ion concentrations at the equatoral crossing altitude of 19000 km versus time. Figure 8b (Bottom panel). Relative concentrations of the hydrogen, oxygen and helium ions versus time. Please note that the colors here represent the three different ions and not the streams of hydrogen as in Figures (3) – (7).

In Figure 8b, we present simulation results that demonstrate the presence of heavier ions (helium and oxygen) during the early hours of refilling. The presence of helium [*Wilford et al.,* 2003] and oxygen [*Nose et al.,* 2018] has been experimentally observed. The helium peak density obtained from our model is larger than the oxygen peak density, which makes physical sense because of oxygen's higher mass. Also, the introduction of time-dependent boundary conditions at the base altitude will keep the fluctuations alive in time and could enhance the presence of heavier ions even further in time. In spite of the simplistic time-independent boundary conditions assumed in this work, the boundary conditions assumed in this work were of the same order of magnitude as observed from the IMAGE satellite data in *Wu et al.* [2003] and *Reinisch et al.* [2004] and as a result, the simulated density profiles were also seen to be similar to the ones included in *Wu et al.* [2003] and *Reinisch et al.* [2004].

Finally in figures (9a) to (9d), we plot the ambipolar electric field between 20 minutes and 40 hours. Consistent with Eq.(3), the spikes in the electric field are a result of the discontinuities in the electron density profile, which is the aggregate of all the ion density profiles. Thus, as expected

in 40 hours, the electric field is seen to decrease significantly with diffusive equilibrium being reached.

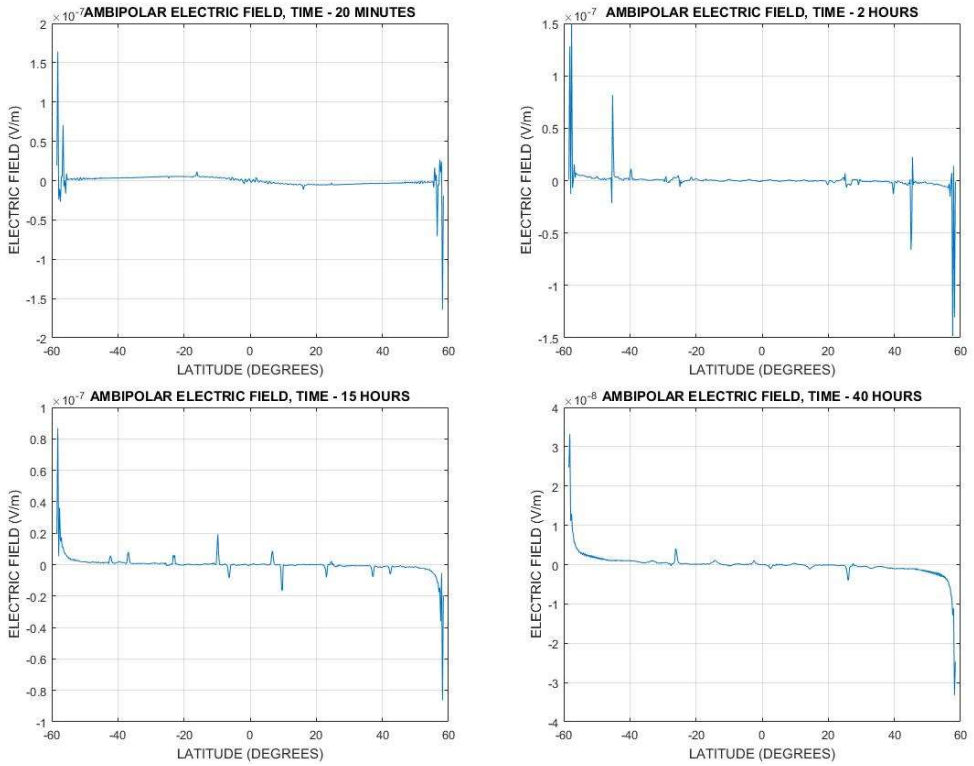

Figures 9a (Top left panel). Ambipolar electric field profile after 20 minutes. Figures 9b (Top right panel). Ambipolar electric field profile after 2 hours. Figures 9c (Bottom left panel). Ambipolar electric field profile after 15 hours. Figures 9d (Bottom right panel). Ambipolar electric field profile after 40 hours.

4 Summary

Summarizing, a multi-ion, two-stream hydrodynamic model has been developed for the plasmasphere refilling problem following a geomagnetic storm. The model predicts high supersonic velocities expected at the onset of refilling, the presence of heavier ions in its early hours, the transition from O^+ to H^+ dominance in the middle stages and correctly estimates the steady-state major ion density after the completion of refilling. The representation of each ion species as two separate streams makes this model philosophically different than other models in the field and remedies the problem of unphysical shock creation at the equator during the early hours of refilling. Our future work will involve the extension of this hydrodynamic model to two and three dimensions as well as the development of a kinetic model which is not predicated on the assumption of Maxwellian velocity distribution functions for the ions.

Acknowledgments

This research was funded primarily in part by Utah/NASA Space Grant Consortium and in part by National Science Foundation Award 1441774 to Utah State University. Additional resources were provided by NASA (Goddard Space Flight Center) through University Space Research Association (USRA) and Sellers Exoplanet Environments Collaboration (SEEC), which is funded

by the NASA Planetary Science Division's Internal Scientist Funding Model. We would like to thank Dr. Alex Glocer (NASA), Dr. George Khazanov (NASA) and Dr. Vladimir Airapetian (NASA/American University) for valuable discussions. No new data has been generated by this work.

References

Bailey G. J., Balan N., & Su, Y. Z. (1997). Sheffield University plasmasphere ionosphere model a review, *Journal of Atmospheric and Terrestrial Physics, 59,* 1541-1552.

Banks, P. M., Nagy A. F., & Axford W. I. (1971). Dynamical behavior of thermal protons in the midlatitude ionosphere and magnetosphere, *Planetary and Space Science, 19,* 1053-1067.

Boris J. P., & Book D. L. (1976). Solution of the continuity equations by the method of flux-corrected transport, *Methods of Computational Physics, 16*, 85-129.

Carpenter, D. L., & Park C. G. (1973). On what ionospheric workers should know about the plasmapause-plasmasphere*, Review of Geophysics, 11,* 133-154.

Darrouzet, F., De Keyser J., & Pierrard V. (Eds.). (2009). *The earth's plasmasphere: A cluster and image perspective*. New York, NY: Springer.

Edde, B. (1992). *Radar: Principles, Technology, Applications,* Upper Saddle River, NJ: Prentice Hall.

Gabor T., Sokolov I. V., Gambosi T. I., Chesney D. R., Clauer C. R., De Zeeuw D. L., et al. (2005). Space Weather Modeling Framework: A new tool for the space science community, *Journal of Geophysical Research: Space Physics, 99(A12)*.

Garrett H. B. (1981). The charging of spacecraft surfaces, *Reviews of Geophysics, 19(4)*, 577-616.

Goldstein, J., Spiro R. W., Reiff P. H., Wolf R. A., Sandel B. R., Freeman J. W., et al. (2002). IMF-driven overshielding electric field and the origin of the plasmasphere shoulder of May 24, *Geophysical Research Letters, 29*, 1819-1822.

Gonzalez, W. D., Joselyn J. A., Kamide Y., Kroehl H. W., Rostoker G., B. T. Tsurutani B. T., & V. M. Vasyliunas (1994). What is a Geomagnetic Storm?, *Journal of Geophysical Research, 99(A4)*, 5771–5792.

Gendrin R. (1975). Waves and wave-particle interactions in the magnetosphere: A review, *Space Science Reviews, 18(2),* 145-200.

Gringauz, K. I. (1963). The structure of ionized gas envelope of Earth from direct measurements in the U.S.S.R of local charged particle concentrations, *Planetary and Space Science, 11*, 281-296.

Hoffmann K. A., & Chiang S. T. (2000*). Computational Fluid Dynamics, Vol. 1*, New York, NY: Engineering Education System.

Huba J. D., & Joyce G. (2000). Sami2 is Another Model of the Ionosphere (SAMI2): A new low-latitude ionosphere model, *Journal of Geophysical Research, 105*, 23035-23053.

Khazanov G. V., Koen M. A., Konnikova Y. V., & Suvorov I. M. (1984). Simulation of ionosphere-plasmasphere coupling considering ion inertia and temperature anisotropy, *Planetary and Space. Science, 32*, 585-598.

Krall J., & Huba J. D. (2013). SAMI3 simulation of plasmasphere refilling, *Geophysical Research Letters, 40*, 2484-2488.

Kuzmin D., Lohner R., & Turek S. (Eds.). (2012). *Flux-corrected transport, Principles, Algorithms and Applications,* New York, NY: Springer.

Maruyuma N., Sun Y., Richards P. G., Middlecoff J., Fang T., Fuller-Rowell T. J. et al. (2016). A new source of the midlatitude ionospheric peak density structure revealed by a new Ionosphere-Plasmasphere model, *Geophysical Research Letters, 43(6)*, 2429-2435.

Millian, R. M., & Thorne R. M. (2007). Review of radiation belt relativistic electron losses, *Journal of Atmospheric and Solar Terrestrial Physics, 69*, 362-377.

Nosé, M., Matsuoka, A., Kumamoto, A., Kasahara, Y., Goldstein, J., Teramoto, M., et al. (2018). Longitudinal structure of oxygen torus in the inner magnetosphere: Simultaneous observations by Arase and Van Allen Probe A. Geophysical Research Letters, 45, 10,177-10,184.

Pirjola R. (2000). Geomagnetically induced currents during magnetic storms, *IEEE Transactions on Plasma Science, 28*, 1867-1873.

Rasmussen C.E., & Schunk R. W. (1988). Multistream hydrodynamic modeling of interhemispheric plasma flow, *Journal of Geophysical Research, 93*, 14557-14565.

Reames D.V. (2017). *Solar Energetic Particles,* Berlin: Springer.

Reinisch B. W., Huang X., Song P., Green J. L., Fung S. F., Vasyliunas V. M. (2004). Plasmaspheric mass loss and refiling as a result of a magnetic storm, *Journal of Geophysical Research, 109(A01202).*

Rishbeth, H., & Garriott O. K. (1969). *Introduction to Ionospheric Physics,* New York, NY: Academic Press.

Sandel, B.R., Goldstein J., Gallagher D. L., & Spasojevic M. (2003). Extreme Ultraviolet Imager Observations of the Structure and Dynamics of the Plasmasphere, *Space Science Reviews, 109*, 25-46.

Schunk R. W. & Nagy A. (2009). *Ionospheres* (pp. 341 344). Cambridge, England: Cambridge University Press.

Schunk R. W., Scherliess L., Sojka J. J., Thomson D. C., Anderson D. N., Codrescu M. et al. (2004). Global Assimilation of Ionospheric Measurements (GAIM), *Radio Science,* 39, https://doi.org/10.1029/2002RS002794.

Scholer M. (1989). Asymmetric time-dependent and stationary magnetic reconnection at the dayside magnetopause, *Journal of Geophysical Research 94(A11)*, 15099-15111

Singh, N., Schunk R. W., & Thiemann H. (1986). Temporal features of the refilling of a plasmaspheric flux tube, *Journal of Geophysical Research, 91*, 13433-13454.

Tu J. -N., Horwitz J. L., Song P., Huang X. -Q., Reinisch, B. W., Richards P. G. (2003). Simulating plasmaspheric field-aligned density profiles measured with IMAGE/RPI: Effects of plasmasphere refilling and ion heating, *Journal of Geophysical Research, 108(A1)*.

Wang Y., Tu J., & Song P. (2015). A new dynamic fluid-kinetic model for plasma transport within the plasmasphere, *Journal of Geophysical Research, 120*, 8486-8502.

Website (*MSIS-E90 Atmosphere Model,* 1990): https://ccmc.gsfc.nasa.gov/modelweb/models/msis_vitmo.php

Website (*Otto,* 2012): http://how.gi.alaska.edu/ao/sim/chapters/chap10.pdf

Wilford C. R., Moffett R. J., Rees J. M., Bailey G. J., & Gonzalez S. A. (2003). Comparison of the He^+ layer observed over Arecibo during solar maximum and solar minimum with CTIP model results, *Journal of Geophysical Research, 108*, 1452-1468.

Young E. R., Torr D. G., & Richards P. G. (1980). A flux preserving method of coupling first and second order equations to simulate the flow of plasma between the plasmasphere and the ionosphere, *Journal of Computational Physics, 38*, 141-156.